Exploring spiral defect chaos in generalized Swift-Hohenberg models with mean flow

A. Karimi

Department of Engineering Science and Mechanics, Virginia Polytechnic Institute and State University, Blacksburg, Virginia 24061, USA

Zhi-Feng Huang

Department of Physics and Astronomy, Wayne State University, Detroit, Michigan 48201, USA

M. R. Paul[*]

Department of Mechanical Engineering, Virginia Polytechnic Institute and State University, Blacksburg, Virginia 24061, USA

We explore the phenomenon of spiral defect chaos in two types of generalized Swift-Hohenberg model equations that include the effects of long-range drift velocity or mean flow. We use spatially extended domains and integrate the equations for very long times to study the pattern dynamics as the magnitude of the mean flow is varied. The magnitude of the mean flow is adjusted via a real and continuous parameter that accounts for the fluid boundary conditions on the horizontal surfaces in a convecting layer. For weak values of the mean flow, we find that the patterns exhibit a slow coarsening to a state dominated by large and very slowly moving target defects. For strong enough mean flow, we identify the existence of spatiotemporal chaos, which is indicated by a positive leading-order Lyapunov exponent. We compare the spatial features of the mean flow field with that of Rayleigh-Bénard convection and quantify their differences in the neighborhood of spiral defects.

I. INTRODUCTION

The chaotic behavior of spatially extended dissipative systems has been intensively studied in recent years [1]. Spatiotemporal chaos has been observed in a wide range of physical systems, including Faraday waves that appear on the surface of an oscillating layer of fluid [2], reacting chemical mixtures [3], excitable media [4], and Rayleigh-Bénard convection in a shallow fluid layer heated from below [1]. In particular, the study of Rayleigh-Bénard convection continues to provide fundamental insights into the dynamics of pattern-forming systems that are driven far from equilibrium [1,5]. The state of spiral defect chaos has received significant attention since its discovery by Morris *et al.* [6]. Spiral defect chaos is characterized by the complex dynamics of rotating spiral defects, and interestingly it occurs for fluid parameters where straight parallel convection rolls are linearly stable [1,5]. Although much effort has been spent on building our understanding of the origins and dynamical features of spiral defect chaos, many open questions still remain.

A significant difficulty in studying spatiotemporal chaos is that the experimental systems of interest are often large and strongly driven. This presents significant obstacles for both analytical and numerical approaches. For example, the numerical simulation of the Boussinesq equations (which govern Rayleigh-Bénard convection) in large domains, for long simulation times, and for many values of the system parameters is out of reach using currently available algorithms and computing resources. Although significant progress has been made in the ability to simulate convection for experimental conditions, the computational cost remains very high [7]. In light of challenges such as these, the use of simpler model equations has played a pivotal role in furthering our physical understanding of spatiotemporal chaos. In Rayleigh-Bénard convection, the two-dimensional Swift-Hohenberg equation [8] has led to numerous physical insights regarding questions of pattern formation [1]. However, the use of the Swift-Hohenberg equation to study spatiotemporal chaos, and in particular spiral defect chaos [9], has been called into question [10], as will be further discussed below. This leaves no clear choice for a model system to be used for the study of spiral defect chaos with direct relevance to fluid convection.

The presence of a long-range mean flow is well known to play an important role in the dynamics of Rayleigh-Bénard convection [1,11,12]. This led to extensions of the Swift-Hohenberg equation to account for these effects [9,13,14]. The mean flow is a weak horizontal flow field that acts over length scales larger than that of the convection rolls; it results from the coupling to fluid vertical vorticity and is induced by roll curvature, amplitude gradients, and wave-number gradients [1,15,16]. The magnitude of the mean flow is much smaller than that of the convective roll motion, making it very difficult to measure in experiment. A typical way to visualize the mean flow in numerical work is to present contours of the integrated horizontal components of the fluid velocity over the depth of the fluid layer [7]. Although the mean flow is weak, it can have a significant effect on the dynamics and stability boundaries of the flow field and also adds a slow time scale to the dynamics. It has been shown numerically that the mean flow is required for spiral defect chaos in Rayleigh-Bénard convection [17].

Spiral defect chaos was initially explored using numerical simulations of the generalized Swift-Hohenberg equation by Xi *et al.* [9]. These simulations were for rather short intervals of time $t \sim 900$, where t is the nondimensional time. For the parameters used, a time of $t = 4.73$ corresponds to the vertical diffusion time of heat τ_v in Rayleigh-Bénard convection [13]. We note that to generate the spiral defect state in this model system, the system needs to be taken far enough from the convective threshold; otherwise, roll-type

----

[*]mrp@vt.edu

patterns would dominate with the system dynamics governed by the motion of topological defects such as grain boundaries, dislocations, and disclinations [18]. Schmitz *et al.* [10] later explored the generalized Swift-Hohenberg equation for the same parameters but for much longer simulation times $t \sim 64\,000$. Their results suggested that the spiral defect state was only a transient with the long-time dynamics characterized by a slow coarsening process to a state dominated by large spirals. This work has cast doubt on the ability of the Swift-Hohenberg equation to exhibit persistent dynamics that resembles spiral defect chaos.

In this paper, we present a careful numerical study of these questions. In particular, we have performed very-long-time simulations ($t = 10^6$ time units) in very large domains, and for a wide range of mean flow strengths. We also compute the leading-order Lyapunov exponent to determine if the dynamics is chaotic. Our investigation is driven by the results on Rayleigh-Bénard convection, which demonstrate the importance of mean flow in spiral defect chaos [5,7].

The remainder of this paper is organized as follows. In Sec. II, we discuss two types of generalized Swift-Hohenberg model equations and provide some details regarding their numerical solution and the computation of the leading-order Lyapunov exponent. In Sec. III, we present our results and discuss the effect of the mean flow on the dynamics. Concluding remarks are given in Sec. IV.

II. APPROACH

A. The generalized Swift-Hohenberg models

A generalized, dimensionless form of the two-dimensional time-dependent Swift-Hohenberg model is given by [9]

$$\frac{\partial \psi}{\partial t} + \mathbf{U} \cdot \nabla \psi = \epsilon \psi - (\nabla^2 + 1)^2 \psi + N[\psi], \quad (1)$$

$$\left[\frac{\partial}{\partial t} - \sigma(\nabla^2 - c^2) \right] \nabla^2 \zeta = g_m [\nabla(\nabla^2 \psi) \times \nabla \psi] \cdot \hat{\mathbf{z}}, \quad (2)$$

where $\psi(x,y,t)$ is a scalar field describing the spatial and temporal variation of the convection patterns, ϵ is a control parameter giving the dimensionless distance from the convective threshold, and $\hat{\mathbf{z}}$ represents the unit vector in the out-of-plane direction. The variable $\zeta(x,y,t)$ is the vertical vorticity potential defined via $\Omega_z = (\nabla \times \mathbf{U})_z = -\nabla^2 \zeta$, where Ω_z is the vertical component of fluid vorticity and $\mathbf{U}$ is the mean flow or drift velocity. ζ can also be interpreted as the stream function for the mean flow, given that

$$\mathbf{U} = \nabla \times (\zeta \hat{\mathbf{z}}) = (\partial_y \zeta, -\partial_x \zeta). \quad (3)$$

In Eq. (2), σ is proportional to the Prandtl number, g_m is a positive real constant that characterizes the mean flow coupling strength, and c is a real parameter introduced for modeling the effect of free-slip ($c = 0$) or no-slip ($c \neq 0$) boundary conditions for the horizontal surfaces of a convection layer. The term $N[\psi]$ in Eq. (1) represents the nonlinearity of the system, which has many different forms in the literature based on system conditions [1,13,19]. In this paper, we present numerical results for two representative cases: (i) $N[\psi] = -\psi^3$ for which the model equations are referred to as the generalized Swift-Hohenberg (GSH) model [19],

and (ii) $N[\psi] = -(|\nabla \psi|^2 \psi + \psi^3)$, for which the equations are referred to as Manneville's model, which was derived in Refs. [13,16] from the Boussinesq equations.

B. Numerical simulations

We numerically integrate Eqs. (1) and (2) using the approach discussed by Cross *et al.* [20] and provide only the essential details here. The domain is a square geometry that is discretized on a spatially uniform grid with periodic lateral boundary conditions. In our numerical simulations, we begin from random initial conditions for ψ and set initially $\zeta(x,y,t = 0) = 0$. We have not performed a detailed study of the long-time dynamics for many different initial conditions due to the computational cost. However, all of our numerical simulations are performed using different random initial conditions, and in the course of analyzing our results we have found no dependence upon the initial conditions. We discretize the spatial domain using a 512×512 grid with a grid spacing of $\Delta x = \Delta y = \lambda_0/8$, where $\lambda_0 = 2\pi$ is the critical wavelength of a convection roll. These parameters are approximately equivalent to a Rayleigh-Bénard system in a box geometry with an aspect ratio of $\Gamma = L/d = 128$, where L is the side length of the box and d is the depth of the convection layer. Each individual simulation is allowed to evolve for $t = 10^6$ time units using a time step of $\Delta t = 0.2$.

The equations are stiff due to the very fast dynamics of the biharmonic operator in comparison to the much slower convective time scale of the pattern dynamics. An efficient solution is obtained using a pseudospectral operator-splitting approach [21]. The linear terms are treated exactly using an explicit exponential time integration [22,23] and the nonlinear terms are evolved forward in time using an explicit predictor-corrector approach. To reduce the contributions of high wave-number modes in the vorticity field, a Gaussian filtering operator F_γ is applied to the right-hand side of Eq. (2) [19]. In Fourier space, it is given by $F_\gamma = \exp(-\gamma^2 q^2/2)$, where γ is the filtering radius and q is the wave number. In our simulations, we have used a filtering radius of $\gamma = \lambda_0/2$.

We compute the leading-order Lyapunov exponent using the standard procedure described in detail in Ref. [24]. The tangent space equations are

$$\frac{\partial \delta\psi}{\partial t} + \mathbf{U} \cdot \nabla \delta\psi + \delta\mathbf{U} \cdot \nabla \psi = \epsilon \delta\psi - (\nabla^2 + 1)^2 \delta\psi$$
$$+ \delta N[\psi, \delta\psi], \quad (4)$$

$$\left[\frac{\partial}{\partial t} - \sigma(\nabla^2 - c^2) \right] \nabla^2 \delta\zeta = g_m [\nabla(\nabla^2 \delta\psi) \times \nabla \psi$$
$$+ \nabla(\nabla^2 \psi) \times \nabla \delta\psi] \cdot \hat{\mathbf{z}}, \quad (5)$$

where $\delta\mathbf{U} = \nabla \times (\delta\zeta \hat{\mathbf{z}})$. The nonlinear term for the GSH equation is

$$\delta N[\psi, \delta\psi] = -3\psi^2 \delta\psi, \quad (6)$$

and for Manneville's model it is

$$\delta N[\psi, \delta\psi] = -(3\psi^2 + |\nabla \psi|^2)\delta\psi - 2[(\nabla \psi) \cdot (\nabla \delta\psi)]\psi. \quad (7)$$

The magnitude of $\delta\psi$ is renormalized after a time t_N to yield a measure of its growth $\|\delta\psi(t_N)\|$, which is used to calculate the instantaneous Lyapunov exponent, i.e.,

$$\tilde{\lambda}_1 = \frac{1}{t_N} \ln \|\delta\psi(t_N)\|. \tag{8}$$

We have used $t_N = 2$ in our simulations. This normalization is repeated in time to generate many values of the instantaneous Lyapunov exponent, whose time average yields the finite-time Lyapunov exponent

$$\lambda_1 = \frac{1}{N_t} \sum_{i=1}^{N_t} \tilde{\lambda}_1, \tag{9}$$

where N_t is the number of renormalizations performed. The limit $N_t \to \infty$ yields the infinite-time Lyapunov exponent.

III. RESULTS

Experimental measurements of spiral defect chaos have typically been performed using large aspect ratio domains, moderate Rayleigh numbers, and compressed gases with a Prandtl number of approximately unity [5]. Generalizations of the Swift-Hohenberg model, as given by Eqs. (1) and (2), have been used to study fundamental features of spiral defect chaos. The choice of the system parameters in the Swift-Hohenberg-type models is important in order to yield dynamics that resembles spiral defect chaos. In order to estimate the appropriate parameters, Xi *et al.* [9] compared a three-mode amplitude equation for the GSH equation with the experimental results of Ref. [25]. Using this approach yielded values of $\sigma = 1$, $\epsilon = 0.7$, and $g_m = 50$. It was also chosen to use $c^2 = 2$, although a specific physical reason for this particular choice is not given. This parameter set has been adopted in most numerical explorations of spiral defect chaos using the Swift-Hohenberg model, including that of Schmitz *et al.* [10], where it was suggested that spiral defect chaos in the numerical simulations was only a transient.

The choice of these system parameters highly affects the magnitude and dynamics of the mean flow. The magnitude of the mean flow is inversely proportional to σ and increases with increasing values of the coupling strength g_m. Cross [26] has presented a careful study of the variation of the dynamics with g_m. For small values of g_m the patterns were dominated by target defects, and for large values of g_m the patterns were dominated by spirals. Schmitz *et al.* [10] computed the appropriate value of g_m based upon the zigzag stability boundary for $\epsilon = 0.7$ and $\sigma = 1$ and found that $g_m \approx 12$. However, it was determined by numerical exploration that a larger value was required to yield dynamics that resembled spiral defect chaos, and a value of $g_m = 50$ was used in their numerics.

Our calculations here indicate an important role played by the parameter c^2 on the strength of mean flows. As described above in Sec. II A, c^2 is related to the choice of boundary conditions on the bottom and top plates of a three-dimensional convection system. Its value physically accounts for the viscous damping that occurs near the horizontal surfaces. A value of $c^2 = 0$ corresponds to perfect slip on the top and bottom plates, and a value of $c^2 \neq 0$ corresponds to a no-slip boundary condition. In the development of the GSH equation [19], the term c^2 is introduced as an unknown constant. In the derivation by Manneville [13,16], c^2 emerges as part of the expansion and averaging procedures used when starting from the Boussinesq equations. Using the nondimensional form of the equations shown in Eqs. (1) and (2) yields a value of $c^2 = 1.03$ (after rescaling) for no-slip boundaries [13]. However, as pointed out in Ref. [13], the precise numerical value of c^2 depends upon the approximation process as well as the manner in which the averaging is done in the vertical direction.

In the following, we have explored the details of the mean flow and the spiral defect state using both Manneville's model and the GSH equation. What separates our work from previous efforts is that we have explored the role of the mean flow by systematically varying the value of c^2 while also computing the leading-order Lyapunov exponent for very-long-time simulations. When using Manneville's model, we have chosen the system parameters to most closely align with those of a Rayleigh-Bénard convection domain exhibiting spiral defect chaos (i.e., $\epsilon = 0.7, \sigma = 2, g_m = 50$). When using the GSH equation, we have used the values commonly used in the literature (i.e., $\epsilon = 0.7, \sigma = 1, g_m = 50$). For both models, we have explored the range of c^2 values from $0.1 \leqslant c^2 \leqslant 4$. We note that for our choice of the system parameters, the Prandtl number is different between our simulations using Manneville's model and the GSH model. Our intention is not to provide a quantitative comparison between these two models, but rather to explore the role of mean flow in spiral defect chaos.

The variation of the mean flow magnitude with c^2 can be quantified by computing the average kinetic energy of the mean flow field. The time-dependent value of the spatially averaged kinetic energy is given by

$$K(t) = \tfrac{1}{2}\langle (U_x^2 + U_y^2)\rangle, \tag{10}$$

where (U_x, U_y) are the x and y components of the mean flow velocity and $\langle \cdots \rangle$ represents the spatial average. In Fig. 1, we plot $\langle K\rangle_t$, which represents the time-averaged value of $K(t)$ as a function of c^2. The time averaging is performed from the data of the final 10^5 time units. The error bars represent the standard deviation of the variation of $\langle K\rangle_t$ about its mean value. The circle symbols are numerical results for Manneville's model and the square symbols are results for the GSH equation. For both models, the data can be fitted to $\langle K\rangle_t \propto c^{-2}$, indicating the rapid increase in the magnitude of the mean flow for decreasing values of c^2.

Figure 2 illustrates the pattern evolution for $c^2 = 2$ using Manneville's model. The value of $c^2 = 2$ is the typical value used in the literature and corresponds to a weak mean flow. At small time $t = 10^3$, the pattern is quite complex and contains many dynamic spiral and defect structures, similar to the scenario given in the simulations of Xi *et al.* [9]. The coarsening to target structures is evidenced by the pattern at $t = 5 \times 10^4$ and represents the approximate duration of the simulations by Schmitz *et al.* using the GSH equation [10]. This coarsening process is extremely slow, as can be seen by comparing the patterns at longer times in Fig. 2 (the pattern at $t = 10^6$ for these simulation parameters is shown in the bottom
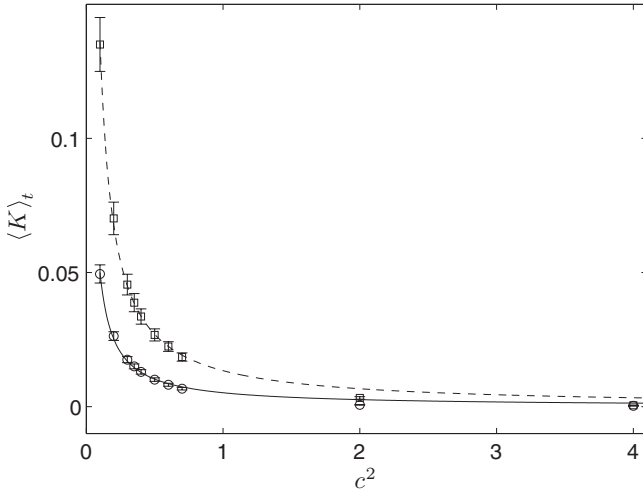
FIG. 1. The variation of the spatial and time-averaged kinetic energy $\langle K \rangle_t$ with c^2. The circle symbols are for Manneville's model with parameters $\epsilon = 0.7$, $\sigma = 2$, $g_m = 50$, and the square symbols are for the GSH equation with $\epsilon = 0.7$, $\sigma = 1$, $g_m = 50$. The lines are curve fits given by $\langle K \rangle_t = 0.013c^{-2}$ for the GSH model and $\langle K \rangle_t = 0.005c^{-2}$ for Manneville's model. The results are averaged using the last 10^5 time units of a simulation with total time $t = 10^6$. The error bars are the standard deviation of the fluctuations of $\langle K \rangle_t$ about its mean value; their maximum values are $\sim 10^{-2}$ and $\sim 10^{-3}$ for the GSH model and Manneville's model, respectively.

right panel of Fig. 3). Note that during the time evolution, some big targets can break up and form small defects, which will then interact and recombine with other targets or spirals, resulting in the process of coarsening.

We have explored the long-time dynamics of the patterns by varying the strength of the mean flow over the parameter range of $0.1 \leqslant c^2 \leqslant 4$. Figure 3 illustrates the patterns at $t = 10^6$ for four different values of c^2. For the cases shown, the patterns resemble the state of spiral defect chaos for $c^2 \lesssim 0.7$, showing spatially complex structures with rapid dynamics of small-scale spirals and localized defects. Although during the evolution process some larger spirals or targets may be formed, they are transients and will soon break up, with new small spiral defects recreated; this procedure will repeat, but no long-lasting, coarsened big targets or spirals can exist. However, for larger c^2 (e.g., $= 2$), the pattern has coarsened to a state dominated by slowly moving target defects, as in the case given in Fig. 2. These observations indicate that strong enough mean flows, as achieved via controlling parameter c^2 in the model equations, are needed to reach a persistent chaotic or dynamic state, not only for breaking up large targets or spirals but also for locally recreating new small spiral-type defects to prevent the coarsening procedure.

To further characterize the properties of system dynamics, in Fig. 4 we examine the time variation of two global quantities: the average kinetic energy $K(t)$ as defined in Eq. (10), and the convective heat flux $J(t)$, which is given by

$$J(t) = \langle \psi^2 \rangle. \tag{11}$$

Figure 4(a) indicates that as the strength of the mean flow increases (i.e., the values of c^2 decrease), the magnitude of
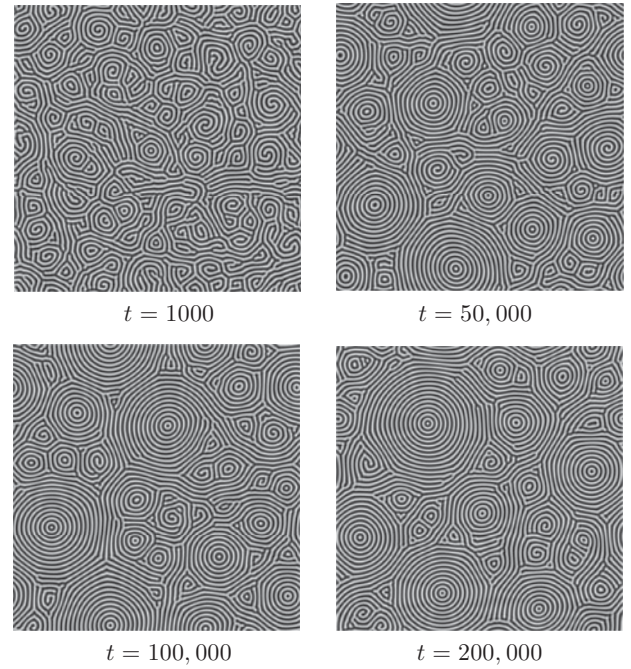

FIG. 2. Instances of the ψ field pattern for Manneville's model with system parameters $\epsilon = 0.7$, $\sigma = 2$, $g_m = 50$, and $c^2 = 2$, showing a slow process of pattern coarsening. Small spiral defects dominate at early times (e.g., $t = 10^3$), whereas at large times the pattern has evolved into a state dominated by large and very slow moving target structures.
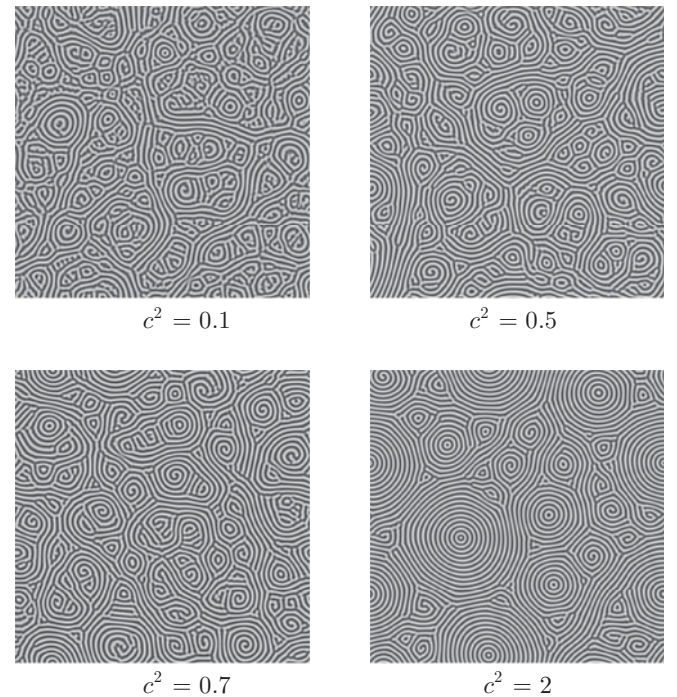

FIG. 3. The long-time patterns for Manneville's model over a range of mean flow strengths as determined by the value of c^2. The simulations are initiated with random initial conditions and are integrated until $t = 10^6$. Other parameters are the same as in Fig. 2.
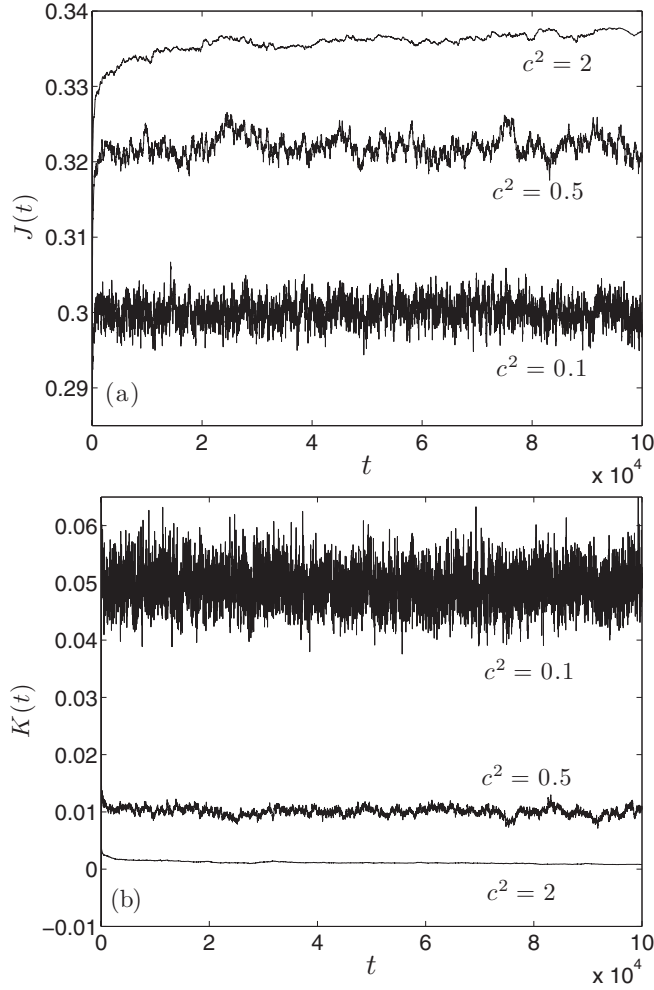
FIG. 4. Time variation of the pattern dynamics in Manneville's model for different magnitudes of the mean flow. The parameters used are the same as those in Fig. 3. (a) Time variation of the convective heat flux $J(t)$ given by Eq. (11); (b) time variation of the average kinetic energy $K(t)$ defined by Eq. (10).

FIG. 5. The variation of the leading-order Lyapunov exponent λ_1 with the magnitude of the mean flow. The value of λ_1 is computed using results for the final 10^5 time units. The circle symbols and the solid line are for Manneville's model using the system parameters $\epsilon = 0.7, \sigma = 2$, and $g_m = 50$. The square symbols and the dashed line are for the GSH equation using the typical system parameters of most previous studies: $\epsilon = 0.7, \sigma = 1$, and $g_m = 50$. The lines are only meant to guide the eye. The error bars represent the standard deviation of λ_1 about its mean value for each value of c^2. The maximum value of the error bar for Manneville's model is $\sim 10^{-3}$ and for the GSH equation is $\sim 10^{-2}$.

the heat flux decreases with increasing fluctuations about the mean value. Such fluctuations are a result of the pattern dynamics. More specifically, the dynamics of the defects yields the excursions to larger and smaller values of the heat flux. For the average kinetic energy as shown in Fig. 4(b), both the magnitude of $K(t)$ and its fluctuations increase with increasing strength of the mean flow. Overall, Fig. 4 can be used to provide some qualitative insight into the complexity of the dynamics. It is clear that for $c^2 = 2$ (which is the parameter used in most previous studies), the disorder in the kinetic energy and heat flux is significantly reduced.

Although global diagnostics such as the kinetic energy and heat flux provide qualitative insights into the complexity of system dynamics, they cannot be used to determine whether the dynamics is chaotic. In order to do so, we have also calculated the finite-time leading-order Lyapunov exponent using the approach discussed in Sec. II B. In Fig. 5, we show the variation of λ_1 with the magnitude of the mean flow, for which $\lambda_1 > 0$ indicates chaos. The circle symbols are the results for Manneville's model, and the solid line is included
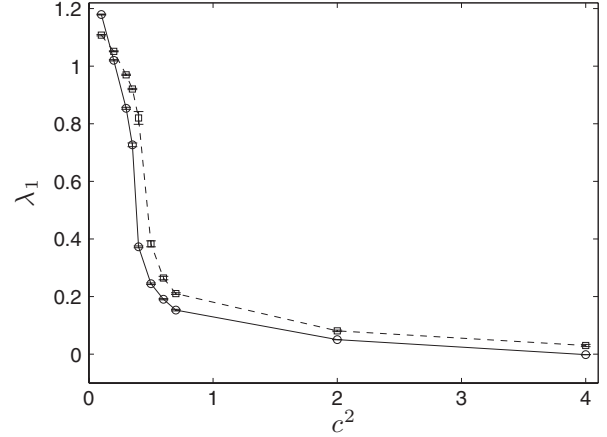
only to guide the eye. We emphasize that these results are obtained from very-long-time simulations to ensure that any slow coarsening dynamics has been captured. The reported values of λ_1 are computed using the final 10^5 time units. The standard deviation of the fluctuations of λ_1 about its mean value is included as error bars. The maximum value of the error bar for the parameters explored is $\sim 10^{-3}$. We have also performed tests on the data in which λ_1 is computed over successive windows of time of various durations to quantify the presence of any slow trends. Our reported values of λ_1 appear to be the converged result, and for the duration of the simulations explored we did not find any indication of slow trends. However, this does not rule out the possibility of even slower dynamics not captured in our simulations.

Our simulations indicate that the dynamics is weakly chaotic for $c^2 \approx 2$, where $\lambda_1 \approx 0.05$. This weak chaos is due to the slow dynamics of the pattern, as can be seen in Fig. 3, where the targets are slowly moving among the more rapid dynamics of defects such as spirals, dislocations, etc. The value of λ_1 increases with the decreasing value of c^2 and thus the increasing magnitude of the mean flow as given in Fig. 5.

We have also included in Fig. 5 the numerical results of the GSH equation to enable a more direct comparison with prior results in the literature. These results are shown as the square symbols and the dashed line. We have allowed c^2 to vary while the remaining parameters are the typical values used in the previous studies: $\epsilon = 0.7, \sigma = 1$, and $g_m = 50$. Overall, our results indicate a very similar trend: the dynamics is weakly chaotic for $c^2 \approx 2$ and becomes increasingly chaotic for smaller c^2 and larger magnitudes of the mean flow. We have performed the same series of tests as for Manneville's model to account for the presence of any slow coarsening process. The

maximum magnitude of λ_1 error bars for the GSH equation is $\sim 10^{-2}$.

Although the connection between the Swift-Hohenberg equations and the Boussinesq equations of Rayleigh-Bénard is phenomenological, a direct comparison between the two can provide further physical insights. In this comparison, we focus mainly on spatial features of the mean flow field for chaotic patterns containing a large number of spiral defects. In Fig. 6(a), we illustrate the relationship between the pattern and the magnitude of the mean flow. The image shown is for Manneville's model at $t = 10^6$ with $c^2 = 0.1$. The dynamics
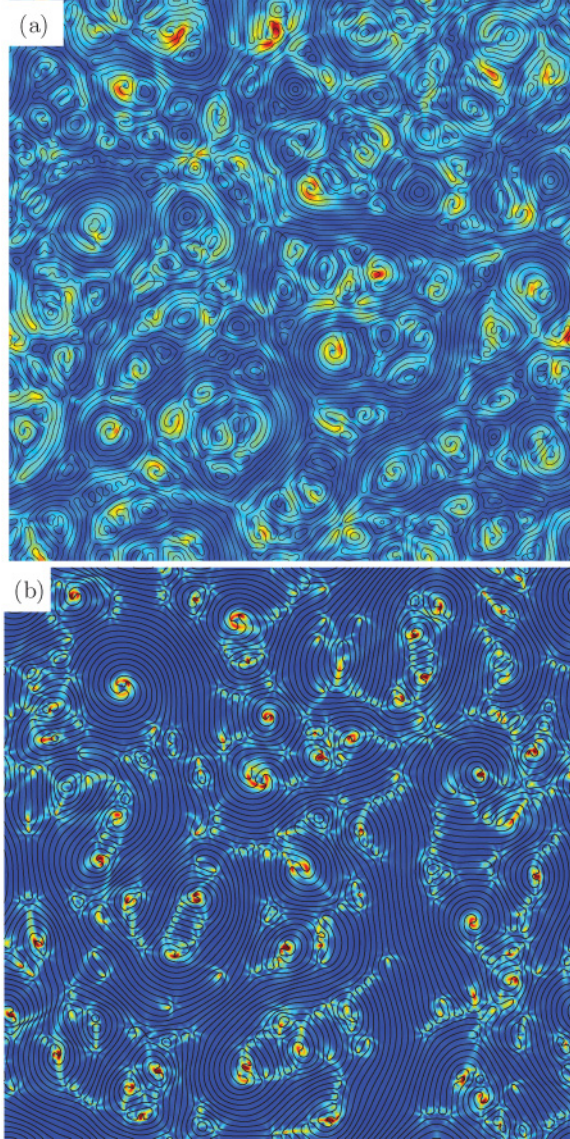

FIG. 6. (Color online) Spatial variation of the mean flow field for chaotic patterns containing many spiral defects. The color contours represent the magnitude of the mean flow field, with red regions (near the spiral cores or defect structures) corresponding to large mean flow magnitude and blue regions (near regions of straight rolls or target structures) corresponding to small mean flow magnitude. The black lines indicate convective roll boundaries. (a) Results for Manneville's equations at $t = 10^6$ using system parameters ($\epsilon = 0.7, \sigma = 2, g_m = 50, c^2 = 0.1$). (b) Results for the Boussinesq equations using system parameters $\epsilon = 0.7$, $\text{Pr} = 1$, and $\Gamma = 128$ at time $t = 232.9$.

is chaotic with $\lambda_1 \approx 1.2$ as given in Fig. 5. The color contours represent the magnitude of the mean flow field $|\mathbf{U}|$, where red indicates regions of large mean flow (located primarily near the cores of spiral defects) and blue indicates regions of small mean flow (located in regions of straight parallel rolls and near target defects). The roll pattern is shown by the black lines, which are given by contours of $\psi = 0$. The mean flow tends to reach its local maximum at locations that contain defect structures and remains large on a length scale of several roll wavelengths around the defect.

We also performed numerical simulations of the three-dimensional time-dependent Boussinesq equations that describe Rayleigh-Bénard convection. We used a parallel spectral approach that is discussed in detail elsewhere (cf. [7]). We have chosen the reduced Rayleigh number $\epsilon = 0.7$, the Prandtl number $\text{Pr} = 1$, and an aspect ratio of $\Gamma = 128$ for the spatial domain. The top and bottom boundaries have the no-slip fluid boundary condition and are held at constant temperature, while periodic boundary conditions are used on the sidewalls. The spatial variation of the mean flow is shown in Fig. 6(b). The mean flow is computed as the vertical average of the horizontal components of the fluid flow field, with red regions indicating large mean flow (near the spiral core) and blue regions corresponding to small mean flow (away from the spiral core). The black lines indicate the contours of the convection rolls. Due to the large aspect ratio of the domain, the computational cost of the numerical simulation is considerable, and the image shown is for a time $t = 232.9$, where t has been nondimensionalized in the usual manner using the time for heat to diffuse across the depth of the layer. Qualitatively, the convective roll pattern is quite similar to what is shown for the Swift-Hohenberg-type equations. The spatial variation of the mean flow field, on the other hand, is different in terms of its rate of decay with the distance from a defect core. The mean flow field is largest at the core regions of the defect structures and decays rapidly with distance away from the defect core. In most cases, the length scale of this decay is approximately that of a single roll [see Fig. 6(b)], as compared to several rolls for results of Manneville's model shown in Fig. 6(a).

The derivation of the Swift-Hohenberg equations is based on a long-wavelength approximation and hence the corresponding results are not expected to be accurate in the core regions of defect structures [8]. This is illustrated in Fig. 7, which shows a close-up view of the mean flow structure near a spiral defect, with panel (a) for results of Manneville's model and panel (b) for the Boussinesq equations. In both cases, the spiral is rotating in a counterclockwise direction. For the Swift-Hohenberg equations, the mean flow exhibits a quadrupole structure centered upon the spiral. The magnitude of the quadrupole is spatially asymmetric and varies with the defect dynamics. The mean flow for the Boussinesq equations is a vortex rotating in the opposite direction to the rotation of the spiral. Our results for the Boussinesq equations are in agreement with those presented by Bodenschatz *et al.* (see Fig. 18 in Ref. [5]).

IV. CONCLUSION

Using generalizations of the Swift-Hohenberg equation, we have explored the spiral defect chaos state and the role
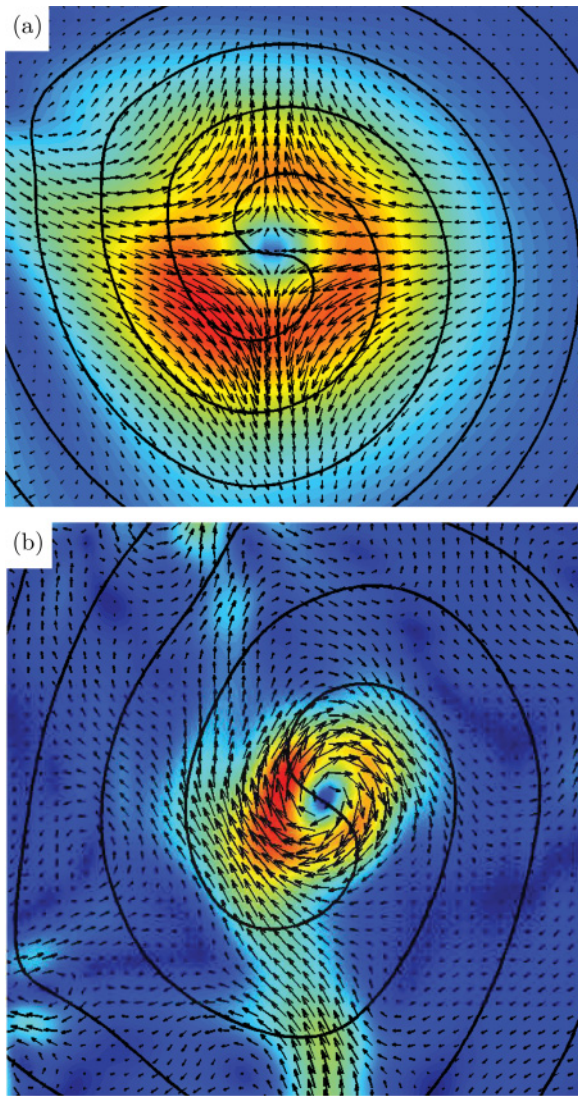
FIG. 7. (Color online) A close-up view of the spatial variation of the mean flow near a spiral defect in a chaotic pattern. The color contours represent the magnitude of the mean flow as in Fig. 6, the black lines indicate the convective roll boundaries, and the arrows are vectors for the mean flow. (a) Results using Manneville's equations with system parameters $\epsilon = 0.7, \sigma = 2$, $g_m = 50$, and $c^2 = 0.4$ at time $t = 7 \times 10^5$. (b) Results from the Boussinesq equations using system parameters $\epsilon = 0.7$, $\sigma = 1$, and $\Gamma = 128$ at time $t = 232.9$.

of the mean flow. Our results show that it is possible to generate chaotic dynamics using Swift-Hohenberg-type model equations that resemble the spiral defect chaos of Rayleigh-Bénard convection. The important insight is that the strength

of the mean flow must be large enough. Reasonable parameter values of ϵ, σ, and g_m that lead to spiral defect chaos have been explored at some length in the previous literature. However, the precise value of parameter c^2 depends on the approximations used in the derivation of Manneville's equations, and the appearance of c^2 is phenomenological in writing down the GSH equations. Our results show that the dynamics varies strongly with the magnitude of c^2, and the commonly used value of $c^2 = 2$ yields a mean flow that is not strong enough to generate persistent dynamics that resembles spiral defect chaos. By choosing a smaller value of c^2, the dynamics is chaotic for as long as we have simulated ($t = 10^6$ time units). Although we focused our discussion on results generated using Manneville's equations, our conclusions and insights also apply to the GSH equations. The particular choice of the form of the nonlinearity does not strongly affect the results in any significant way that we have found. The necessity of a strong enough mean flow to support spiral defect chaos is in agreement with what has been found from the Boussinesq equations [17].

However, there are significant differences between numerical results from the Swift-Hohenberg-type model equations and those generated using the full three-dimensional Boussinesq equations. The Swift-Hohenberg equations are not expected to capture the small-scale features correctly due to the long-wavelength approximation involved, and we have quantified some aspects of this by comparing the mean flow fields around a single spiral defect.

We anticipate that our results will have several uses. First is that Swift-Hohenberg-type equations can be used as a model to study spatiotemporal chaos in a system with direct relevance to fluid phenomena such as Rayleigh-Bénard convection. This is a significant advantage since numerical simulations of the Boussinesq equations are computationally very expensive [7]. The Swift-Hohenberg model equations could be used to explore fundamental ideas of spatiotemporal chaos that are currently inaccessible to the full fluid equations. Examples include a detailed study of microextensivity [27,28] or the computation of the characteristic Lyapunov exponents [29,30]. In addition, our comparison of the spatial variation of the mean flow around spiral defect core structures could be used to guide the development of more accurate theoretical descriptions of spiral defect chaos.

[1] M. C. Cross and P. C. Hohenberg, Rev. Mod. Phys. **65**, 851 (1993).

[2] J. Gollub and R. Ramshankar, in *New Perspectives in Turbulence*, edited by L. Sirovich (Springer-Verlag, New York, 1991), p. 165.

[3] G. S. Skinner and H. L. Swinney, Physica D **48**, 1 (1991).

[4] M. Bar and M. Eiswirth, Phys. Rev. E **48**, R1635 (1993).

[5] E. Bodenschatz, W. Pesch, and G. Ahlers, Annu. Rev. Fluid Mech. **32**, 709 (2000).

[6] S. W. Morris, E. Bodenschatz, D. S. Cannell, and G. Ahlers, Phys. Rev. Lett. **71**, 2026 (1993).

[7] M. R. Paul, K.-H. Chiam, M. C. Cross, P. F. Fischer, and H. S. Greenside, Physica D **184**, 114 (2003).

[8] J. Swift and P. C. Hohenberg, Phys. Rev. A **15**, 319 (1977).

[9] H. W. Xi, J. D. Gunton, and J. Viñals, Phys. Rev. Lett. **71**, 2030 (1993).

[10] R. Schmitz, W. Pesch, and W. Zimmermann, Phys. Rev. E **65**, 037302 (2002).

[11] A. C. Newell, T. Passot, and M. Souli, J. Fluid Mech. **220**, 187 (1990).

[12] A. C. Newell, T. Passot, and M. Souli, Phys. Rev. Lett. **64**, 2378 (1990).

[13] P. Manneville, in *Cellular Structures in Instabilities*, edited by J. Wesfreid and S. Zaleski, Vol. 210 (Springer-Verlag, Berlin, 1984), pp. 137–155.

[14] M. C. Cross and Y. Tu, Phys. Rev. Lett. **75**, 834 (1995).

[15] E. D. Siggia and A. Zippelius, Phys. Rev. Lett. **47**, 835 (1981).

[16] P. Manneville, J. Phys. **44**, 759 (1983).

[17] K.-H. Chiam, M. R. Paul, M. C. Cross, and H. S. Greenside, Phys. Rev. E **67**, 056206 (2003).

[18] Z.-F. Huang and J. Viñals, Phys. Rev. E **75**, 056202 (2007).

[19] H. S. Greenside and M. C. Cross, Phys. Rev. A **31**, 2492 (1985).

[20] M. C. Cross, D. Meiron, and Y. Tu, Chaos **4**, 607 (1994).

[21] C. Canuto, A. Quateroni, and T. Zang, *Spectral Methods in Fluid Dynamics* (Springer-Verlag, Berlin, 1988).

[22] S. M. Cox and P. C. Matthews, J. Comput. Phys. **176**, 430 (2002).

[23] A.-K. Kassam and L. N. Trefethen, SIAM J. Sci. Comput. **26**, 1214 (2005).

[24] A. Wolf, J. Swift, H. L. Swinney, and A. Vastano, Physica D **16**, 285 (1985).

[25] E. Bodenschatz, J. R. de Bruyn, G. Ahlers, and D. S. Cannell, Phys. Rev. Lett. **67**, 3078 (1991).

[26] M. C. Cross, Physica D **97**, 65 (1996).

[27] S. Tajima and H. S. Greenside, Phys. Rev. E **66**, 017205 (2002).

[28] A. Karimi and M. R. Paul, Chaos **20**, 043105 (2010).

[29] F. Ginelli, P. Poggi, A. Turchi, H. Chatè, R. Livi, and A. Politi, Phys. Rev. Lett. **99**, 130601 (2007).

[30] D. Pazó, I. G. Szendro, J. M. López, and M. A. Rodríguez, Phys. Rev. E **78**, 016209 (2008).